

AEROELASTIC ANALYSIS OF TYPICAL SECTIONS WITH STRUCTURAL AND AERODYNAMIC NONLINEARITIES

E. Camilo*, F. D. Marques*, J. L. F. Azevedo**

*University of São Paulo - Engineering School of São Carlos - São Carlos - SP, Brazil,

**Aerospace Technical Center, Aeronautics and Space Institute - São J. dos Campos - SP, Brazil

Keywords: *nonlinear aeroelasticity, CFD methods, Euler equations, transonic flows, LCO*

Abstract

The application of time domain analyses for aeroelastic problem in a transonic flow is considered. The methodology here proposed is to present an investigation on the effects of nonlinearities on aeroelastic behavior for an airfoil moving in pitch and plunge. Here structural dynamics is considered in terms of concentrated nonlinearities. The CFD tool employed in the present work is based on the Euler formulation. The governing equations are integrated by cell-centered, finite-volume, centered space discretization and five-stage, hybrid, explicit, Runge-Kutta time marching scheme. This CFD tool solves flows around two-dimensional lifting surfaces moving in pitch and plunge. The computational domain is discretized using unstructured grids and the movement is modeled with dynamic mesh algorithm. To solve the aeroelastic problem the Runge-Kutta method is applied combined with the CFD code. The time domain aeroelastic responses concerned particularly the NACA0012 airfoil are analysed by investigating typical LCO nonlinear effects from phase plane.

1 Introduction

In the last decades, nonlinear dynamics analysis has been largely developed and explored, both in the theoretical and experimental point of view, in a vast diversity of fields in science and engineering. Nonlinear aeroelasticity is a multidisci-

plinary field, that is very important in aeronautics and aerospace engineering [10]. Most aeroelastic analyses of flight vehicles have been performed under the assumption of linearity. Under this assumption, the characteristics of flutter and divergence can be obtained. However, the influence of nonlinearities on modern aircraft is becoming increasingly important and the requirement for more accurate predictive tools grows stronger [16].

There are two possible consequences of any nonlinear effect. One is that exponentially growing oscillations predicted by an unstable linear model are attenuated due to the nonlinear effects, finite amplitude, steady-state oscillation. Limit cycle oscillations (LCOs) have been a persistent problem on several fighter aircraft designs and wind-tunnel models, where it can be generally encountered on external store configurations. [7,8]. LCO may be beneficial because the nonlinearity reduces the amplitude of the oscillations. Of course, structural integrity may still be an issue if the LCO amplitudes are too large. The second consequence is wholly detrimental. In this instance, a system that may be stable to a sufficiently small perturbation, can become unstable due to a large disturbance [9].

LCO in aeroelastic systems appear to be more prevalent in transonic flow than in subsonic flow. Aerodynamic nonlinearity is associated with the presence of shock waves in transonic flows. In this situation, the unsteady forces generated by motion of the shock wave have been shown to destabilize single degree-of-freedom airfoil

pitching motion and affect the bending-torsional flutter by lowering the flutter speed at the so-called transonic dip phenomenon. Of course, nonlinear structural mechanisms can also lead to LCO whether the flow is transonic or not. There have designed to exhibit LCO due to a structural nonlinearity, and such test results have been successfully correlated with analysis. However, the present understanding of LCO induced by aerodynamic nonlinearities is less complete, and no systematic quantitative correlation between theory and experiment has been achieved [20].

Computational aeroelasticity is a relatively new field emphasizing those types of aeroelastic problems where loads based on Computational Fluid Dynamics (CFD), which can be both unsteady and nonlinear, are used [10,11,18]. A significant amount of effort devoted towards the numerical solution of transonic aeroelastic phenomena, not only in the prediction of transonic dip effects [3,4], but also towards that of LCO. Euler and Navier-Stokes schemes have been coupled with structural models [1,13,14,18].

The methodology here presented, which is based on the ideas of [1,14] intend to obtain the time domain aeroelastic responses for an airfoil moving in pitch and plunge in the transonic regime. The CFD tool has been achieved in cooperation with CTA/IAE group [2,5,18,19]. This CFD tool has been tested and developed for the several aerodynamic and aeroelastic applications considered in the CTA/IAE. However this CFD tool had never used for time domain aeroelastic analyses before.

In the CFD code the Euler equations are integrated by cell-centered, finite-volume, centered space discretization and five-stage, hybrid, explicit, Runge-Kutta time marching scheme. This CFD tool solves flows around two-dimensional lifting surfaces moving in pitch and plunge. The computational domain is discretized using unstructured grids and the movement is modeled with dynamic mesh algorithm. To solve the aeroelastic problem the Runge-Kutta method is applied combined with the CFD code. The time domain aeroelastic responses concerned particularly the NACA0012 airfoil are analysed by in-

vestigating typical nonlinear effects like LCO from phase plane.

2 Aerodynamic Simulation

In the present study, the flow was assumed to be governed by the two-dimensional, time-dependent Euler equations, which may be written in integral form for Cartesian coordinates as:

$$\frac{\partial}{\partial t} \int_{\mathbf{V}} \mathbf{Q} dx dy + \int_{\mathbf{S}} (\mathbf{E} dy - \mathbf{F} dx) = 0, \quad (1)$$

where \mathbf{V} represents the area of the control volume and \mathbf{S} is its boundary, \mathbf{Q} is the vector of conserved quantities and the inviscid flux vectors, \mathbf{E} and \mathbf{F} , are given by:

$$\mathbf{Q} = \begin{bmatrix} \rho \\ \rho u \\ \rho v \\ e \end{bmatrix}, \quad \mathbf{E} = \begin{bmatrix} \rho U \\ \rho u U + p \\ \rho v U \\ (e + p)U + x_t p \end{bmatrix},$$

$$\mathbf{F} = \begin{bmatrix} \rho V \\ \rho v V \\ \rho v V + p \\ (e + p)V + y_t p \end{bmatrix}. \quad (2)$$

where ρ , u , v , p and e are density, the two Cartesian components of the velocity, the pressure, and the specific total energy, respectively.

The contravariant velocity components are defined as:

$$U = u - x_t, \quad V = v - y_t, \quad (3)$$

where x_t and y_t represents the Cartesian velocity components of the mesh.

Pressure is represented by the following state equation:

$$p = (\gamma - 1) \left[e - \frac{1}{2} \rho (u^2 + v^2) \right] \quad (4)$$

where γ is the ratio of specific heats.

The Euler equations can be rewritten for each i -th control volume as:

$$\frac{\partial}{\partial t} (V_i \mathbf{Q}_i) + \int_{S_i} (\mathbf{E} dy - \mathbf{F} dx) = 0. \quad (5)$$

The Euler equations are a set of nondissipative hyperbolic conservation laws. Hence, their numerical solution requires the introduction of artificial dissipation terms in order to avoid oscillations near shock waves and to damp high frequency uncoupled error modes. The numerical dissipation terms are formed as a careful blend of undivided Laplacian and biharmonic operators [19]. Hence, the artificial dissipation operator, D_i , can be written as,

$$D_i = d^2(\mathbf{Q}_i) - d^4(\mathbf{Q}_i), \quad (6)$$

where $d^2(\mathbf{Q}_i)$ represents the contribution of the undivided Laplacian operator, and $d^4(\mathbf{Q}_i)$ the contribution of the biharmonic operator. The biharmonic operator is responsible for providing the background dissipation to damp high frequency uncoupled error modes and the undivided Laplacian artificial dissipation operator prevents oscillations near shock waves [5].

Therefore, the Euler equations after be fully discretized in space and the explicit addition of artificial dissipation terms, can be written as:

$$\frac{d}{dt}(V_i \mathbf{Q}_i) + C(\mathbf{Q}_i) - D(\mathbf{Q}_i) = 0, \quad (7)$$

where $C(\mathbf{Q}_i)$ represents convective operator, given by:

$$\int_{S_i} (\mathbf{E}dy - \mathbf{F}dx) \approx C(\mathbf{Q}_i) = \sum_{k=1}^3 [\mathbf{E}(\mathbf{Q}_{ik})(y_{k2} - y_{k1}) - \mathbf{F}(\mathbf{Q}_{ik})(x_{k2} - x_{k1})], \quad (8)$$

where

$$\mathbf{Q}_{ik} = \frac{1}{2}(\mathbf{Q}_i + \mathbf{Q}_k), \quad (9)$$

and the (x_{k1}, y_{k1}) and (x_{k2}, y_{k2}) are vertices which define the interface between the volumes i and k .

The unsteady Euler code is based on Jamenson's finite volume and Runge-Kutta time-marching using a second-order accurate, 5-stage, explicit, hybrid scheme. The 2-D Euler equations in integral form are discretized by a finite volume procedure in an unstructured mesh [18].

2.1 Equations of motion

Consider a typical two-degrees-of-freedom (DOF) airfoil section as shown in Fig.1. The equations of motion of this aeroelastic system can be written in the form [6]:

$$m\ddot{w} - S_\alpha \ddot{\alpha} + \bar{G}(w) = -L, \quad (10)$$

$$-S_\alpha \ddot{w} + I_\alpha \ddot{\alpha} + \bar{M}(\alpha) = M_{ea}. \quad (11)$$

where the right-hand-side terms represent the aerodynamic loading terms, which are obtained from CFD code. The left-hand-side terms m , S and I_α are the airfoil mass, airfoil static moment and pitch axis moment of inertia about elastic axis, respectively. $\bar{G}(w) = k_w w$ and $\bar{M}(\alpha) = k_\alpha \alpha$ are the nonlinear plunge and pitch stiffness terms.

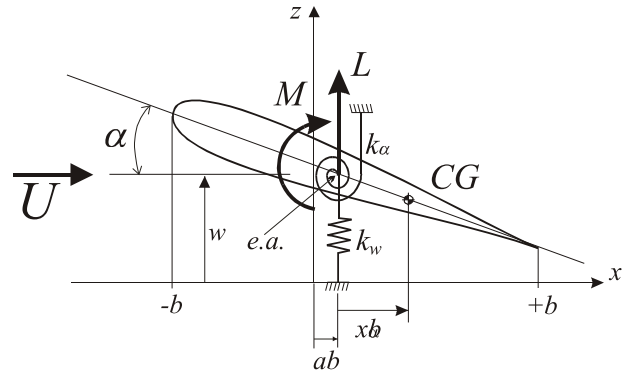


Fig. 1 Typical section model.

The constant k_w is the spring constant for the plunging motion and k_α is the nonlinear spring stiffness related to the pitching motion. Several classes of nonlinear stiffness contributions have been studied in papers treating the open-loop dynamics of aeroelastic system [13,14]. In this work, k_α is kept linear with respect to w , but k_α is represented as the following polynomial function of α , that is:

$$k_\alpha = k_{\alpha_0} + k_{\alpha_1} \alpha + k_{\alpha_2} \alpha^2 + k_{\alpha_3} \alpha^3 + \dots \quad (12)$$

The aeroelastic system given by Eqs. (10) and (11) are rewritten as a system of first-order differential equations by setting:

$$\phi_1 = \frac{w}{b}; \quad \phi_2 = \frac{\dot{w}}{b}; \quad \phi_3 = \alpha; \quad \phi_4 = \dot{\alpha}, \quad (13)$$

with

$$\phi = [\phi_1 \quad \phi_2 \quad \phi_3 \quad \phi_4], \quad (14)$$

where w and α are airfoil vertical displacement and pitch DOF, respectively and b is airfoil semi-chord. The system of aeroelastic equations is expressed as:

$$\dot{\phi} = \mathcal{K}(\phi, C_L, C_m, U^*), \quad (15)$$

where \mathcal{K} is a nonlinear function of ϕ , C_L and C_m are lift and pitch moment coefficient, and U^* is the reduced velocity. The fourth-order Runge-Kutta time-stepping scheme is used for the differential aeroelastic equations (Eqs. (15)).

3 Time-Marching Aeroelastic Analysis

The results were calculated by first computing a converged steady flow solution about the airfoil with angle 0.1 degree of pitching about the elastic axis. The steady Euler solution was determined using the steady portion of the original unsteady Euler solver.

The subsequent aeroelastic response of the model was obtained by a time marching solution of the aeroelastic equations. The coupled computational fluid dynamic (CFD) and computational structural dynamics (CSD) method to the two-dimensional typical section was performed. It consists of a NACA0012 airfoil.

Time integration of the coupled fluid-structural equations of motion (Eq. (15)) is applied and incorporated within the CFD Euler code as follows:

1. At time level n , perform an iteration of the Euler equation and calculate values for C_L and C_m ;
2. This information is used by the equations of motion to determine the position and velocity of the airfoil;
3. The new position and velocity are taken into account by the flow equations, and the process is repeated.

The solutions were determined on an unstructured mesh that moved with the airfoil. To examine the effect of aerodynamic nonlinearities about the NACA0012 airfoil the following parameter related to the linear structure (typical section) were chosen:

$$x_\alpha = 1.8, \quad r_\alpha^2 = 3.48, \quad \bar{\omega} = 1, \\ \mu = 60, \quad a = -0.25.$$

where r_α is airfoil radius of gyration about elastic axis, x_α is nondimensional distance from elastic axis to mass center, $\bar{\omega} = \frac{\omega_w}{\omega_\alpha}$ where ω_w and ω_α are uncoupled natural frequency of bending and torsion modes, a is location of elastic axis and μ is airfoil-fluid mass ratio.

Different Mach numbers and values of the reduced velocity, $U^* = \frac{U_\infty}{b\omega_\alpha}$, where U_∞ is the freestream velocity, b is the airfoil half-chord and ω_α is the pitch natural frequency, were considered for simulations. At a constant Mach number 0.9, a series of time integrations was performed at increasing reduced velocities. Figure 2 and 3 presents a simulation for $U^* = 35$, where the system approaches the stable equilibrium point. Figure 4 and 5 shows divergent response system for $U^* = 45$, opposingly to the results in Fig. 2 and 3.

In between these two U^* conditions, there must be a particular point where the system is neutrally stable. This is shown in Fig. 6 and 7, when $U^* = 40$. However, most of the runs do not need computations for many time periods, because system oscillations were easily identified with diverging or converging amplitude by looking at only few of them.

Time integration for Mach number 0.85 were performed. Below a reduced velocity of $U^* = 25$, the system has presented an oscillatory mode with low amplitude. The results are shown in the Fig. 8 and 9, where it can be seen that the system first stabilizes in equilibrium point (*cf.* Fig. 8) for $U^* = 10$ and limit cycle oscillations (*cf.* Fig. 9) for $U^* = 23$. For reduced velocities above 23 to nearly 40, the system shows apparent divergent response as depicted in Fig. 10 and 11 for $U^* = 30$ and $U^* = 40$. In Fig. 12 and 13, for $U^* = 50$, the system reaches a higher frequency oscillatory mode with slightly increasing amplitude.

AEROELASTIC ANALYSIS OF TYPICAL SECTIONS WITH STRUCTURAL AND AERODYNAMIC NONLINEARITIES

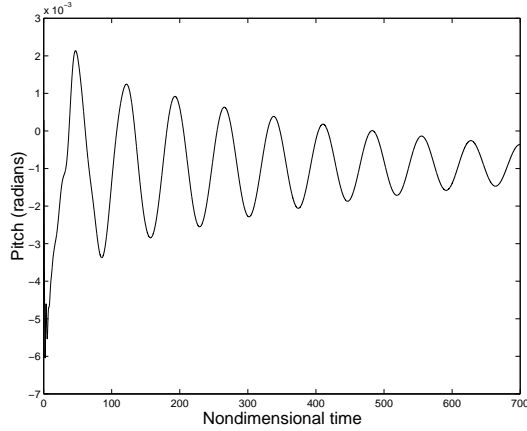


Fig. 2 Time history (damped response), $M = 0.9$ and $U^* = 35$.

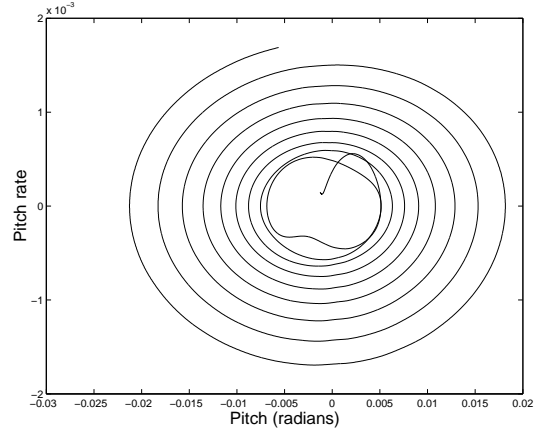


Fig. 5 Phase plane (divergent response), $M = 0.9$ and $U^* = 45$.

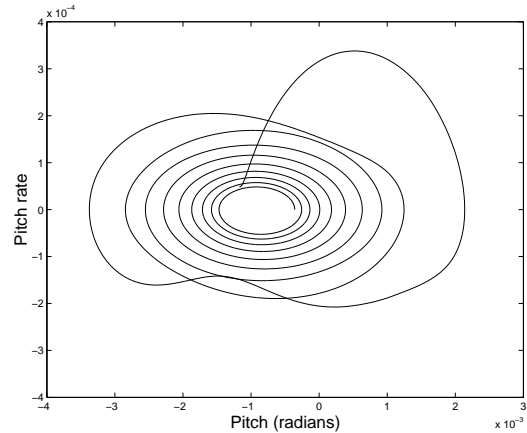


Fig. 3 Phase plane (damped response), $M = 0.9$ and $U^* = 35$.

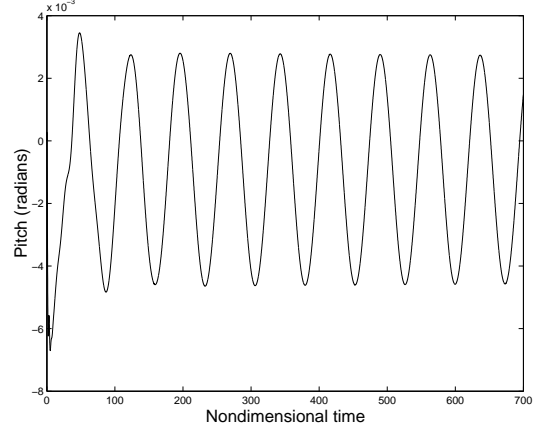


Fig. 6 Time history, $M = 0.9$ and $U^* = 40$.

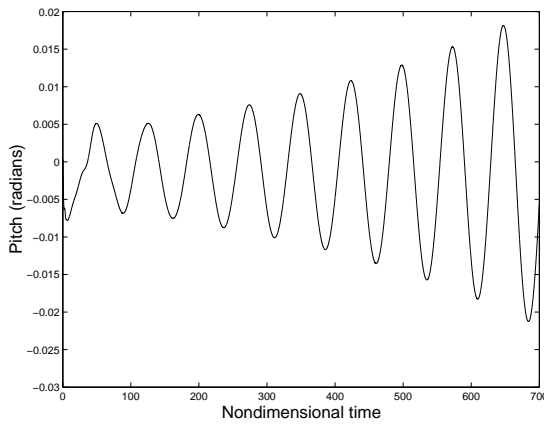


Fig. 4 Time history (divergent response), $M = 0.9$ and $U^* = 45$.

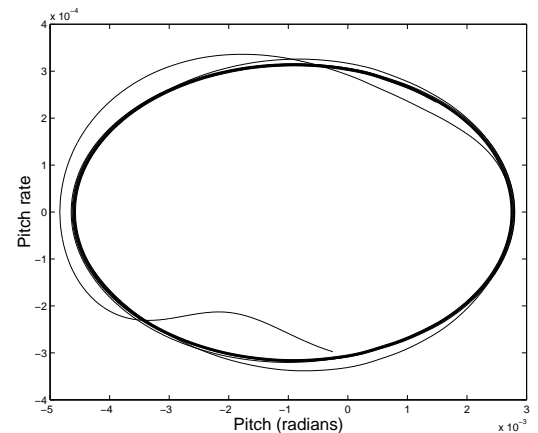


Fig. 7 Phase plane, $M = 0.9$ and $U^* = 40$.

a steady oscillatory motion.

Polynomial nonlinearity given by:

$$k_\alpha = 0.18 + 18000\alpha^2 - 98000000\alpha^4 \quad (16)$$

For $U^* = 65$ (Fig. 14 and 15) the system initially shows diverging behaviour but then reaches

was then added to the torsional spring, and the new coupled system was integrated. In Fig. 16 and 17 the pitch time history and phase plane trajectory for Mach number 0.85 and $U^* = 65$ are shown. Note the obvious distorted character of the phase plane, indicating the influence of structural nonlinearities in the solution. For $U^* = 75$ the system has presented LCO behavior, but with two amplitudes (*cf.* Fig. 18 and 19). In all cases, for $M = 0.85$ with linear structure, LCO amplitudes increase with the reduced velocity, where it seems to take the form of a supercritical bifurcation.

For reduced velocities above 80, the system experiences strong divergence conditions, with the results shown in Fig. 20. It can be noted, in comparison with the approach to limit cycles seen previously, that the divergence is extremely intense.

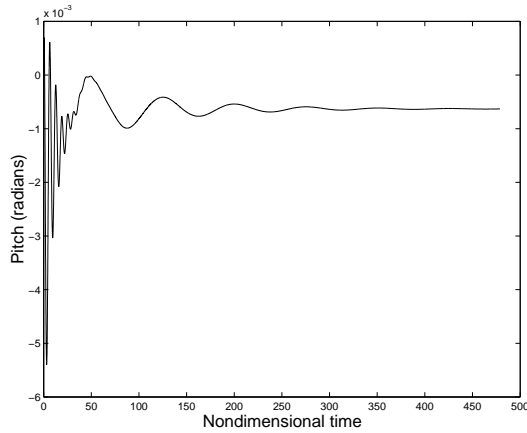


Fig. 8 Time history, $M = 0.85$ and $U^* = 10$.

Simulations when structural nonlinearities are included to the aeroelastic system were also performed for the following parameter:

$$x_\alpha = 0.2, \quad r_\alpha^2 = 0.29, \quad \bar{\omega} = 0.34335, \\ \mu = 60, \quad a = -0.2.$$

Figures 21 to 24 illustrate the pitching response for the NACA 0012 airfoil in transonic flow ($M=0.85$) and reduced velocity of 2. Figure 21 and 22 presents the response when linear structure is considered, while in Figure 23 and 24

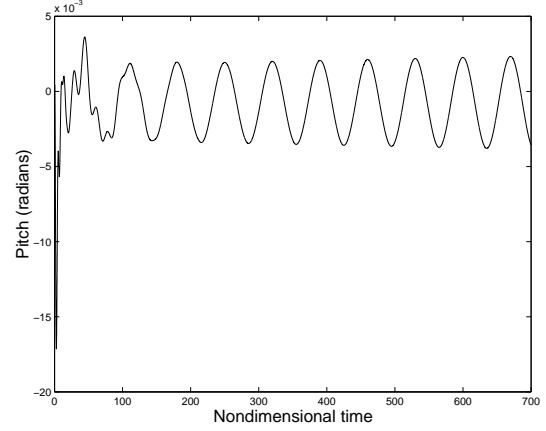


Fig. 9 Time history, $M = 0.85$ and $U^* = 23$.

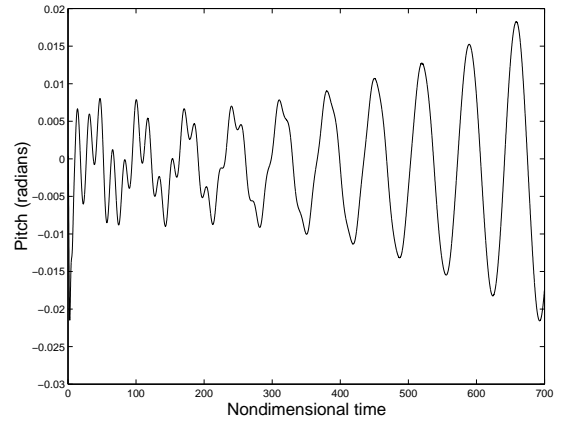


Fig. 10 Time history, $M = 0.85$ and $U^* = 30$.

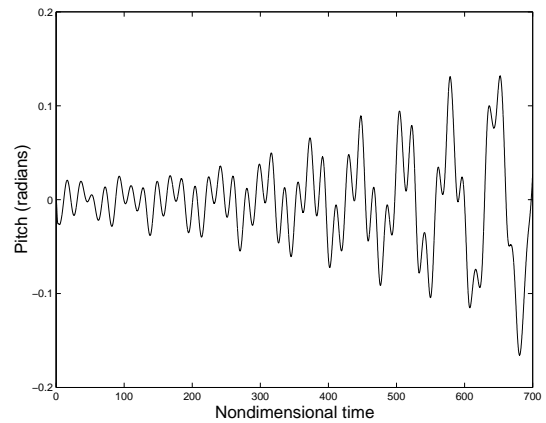


Fig. 11 Time history, $M = 0.85$ and $U^* = 40$.

a polynomial nonlinearity (Eq. (16)) is assumed to the pitching stiffness.

AEROELASTIC ANALYSIS OF TYPICAL SECTIONS WITH STRUCTURAL AND AERODYNAMIC NONLINEARITIES

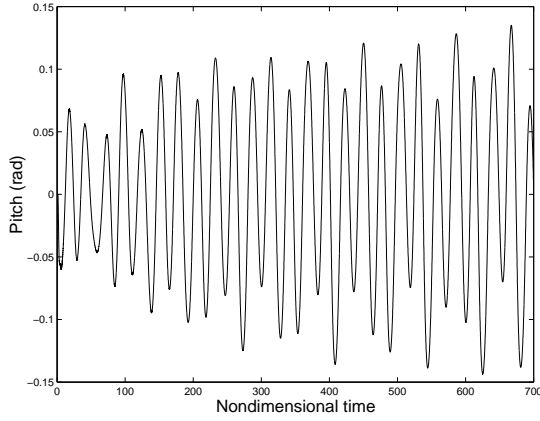


Fig. 12 Time history, $M = 0.85$ and $U^* = 50$.

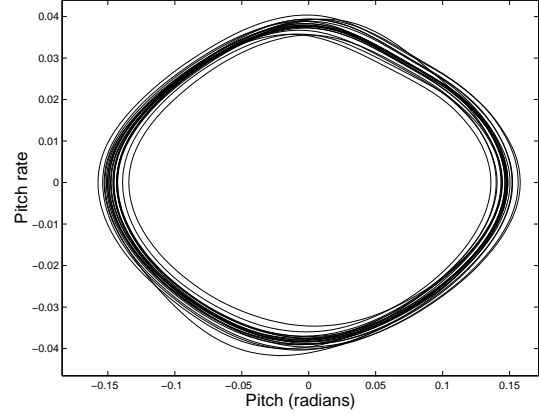


Fig. 15 Phase plane without polynomial structural nonlinearity, $M = 0.85$ and $U^* = 65$.

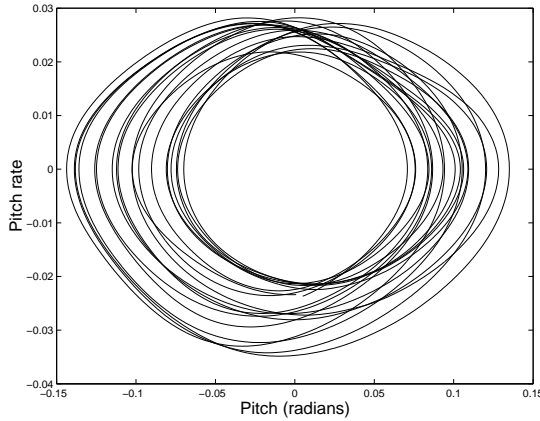


Fig. 13 Phase plane, $M = 0.85$ and $U^* = 50$.

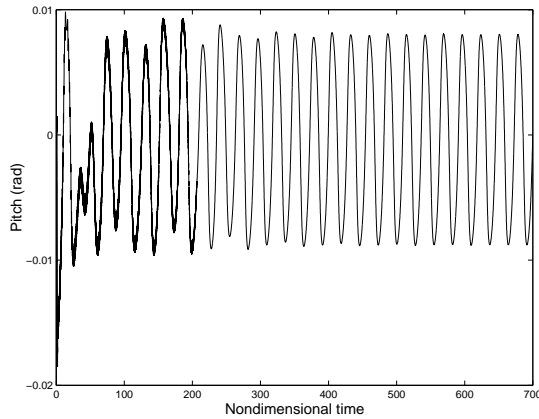


Fig. 16 Time history with polynomial structural nonlinearity, $M = 0.85$ and $U^* = 65$.

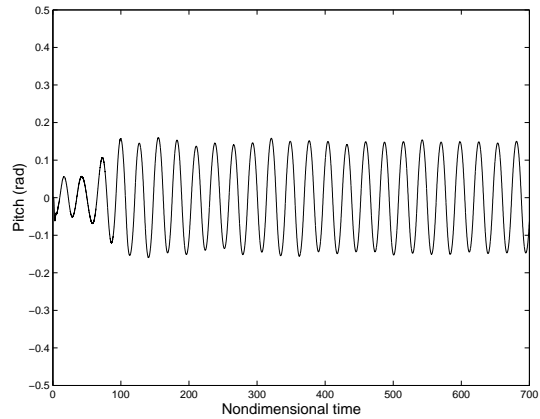


Fig. 14 Time history without polynomial structural nonlinearity, $M = 0.85$ and $U^* = 65$.

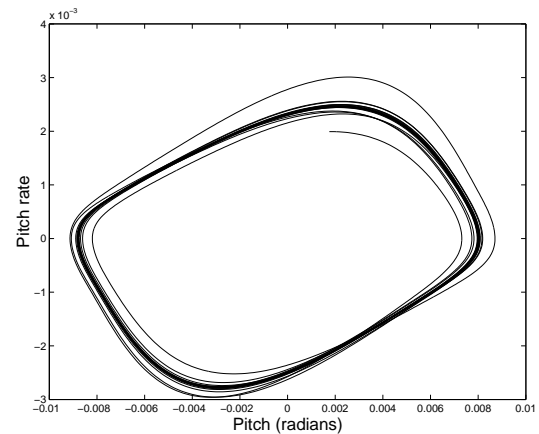


Fig. 17 Phase plane with polynomial structural nonlinearity, $M = 0.85$ and $U^* = 65$.

4 Conclusions

An integrated fluid-structure simulation program has been developed for a simulation of nonlinear

aeroelastic response behavior in transonic regime with nonlinear structural parameters. This pro-

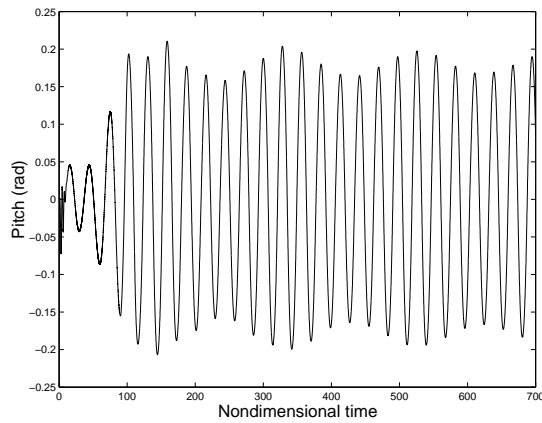


Fig. 18 Time history, $M = 0.85$ and $U^* = 75$.

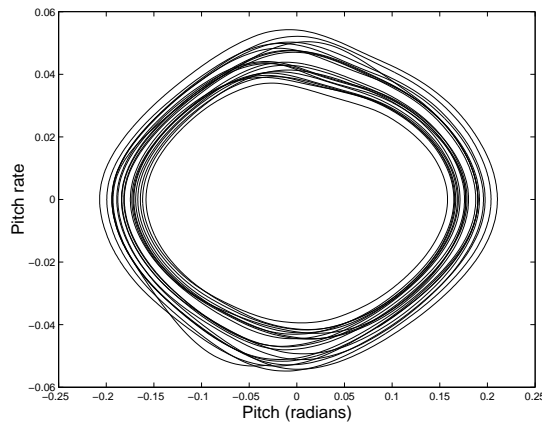


Fig. 19 Phase plane, $M = 0.85$ and $U^* = 75$.

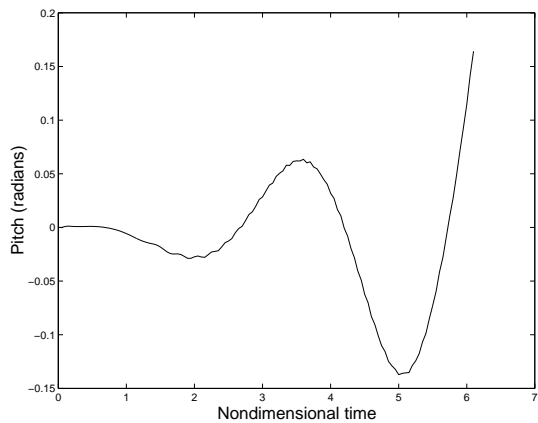


Fig. 20 Time history, $M = 0.85$ and $U^* = 80$.

gram consists of an aerodynamic model given by two-dimensional unsteady Euler solver and dynamic grid deformation code. To solve the aeroelastic problem the Runge-Kutta method is applied combined with the CFD code. The coupled

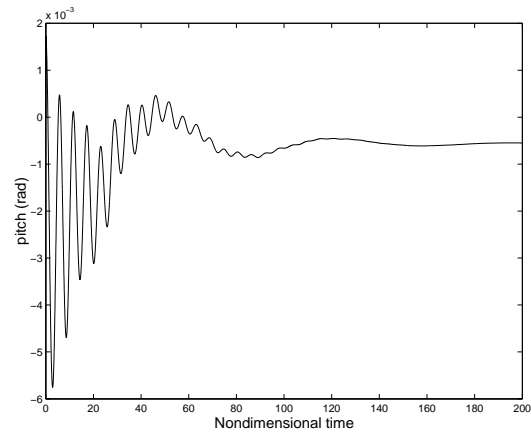


Fig. 21 Time history without polynomial structural nonlinearity, $M = 0.85$ and $U^* = 2$.

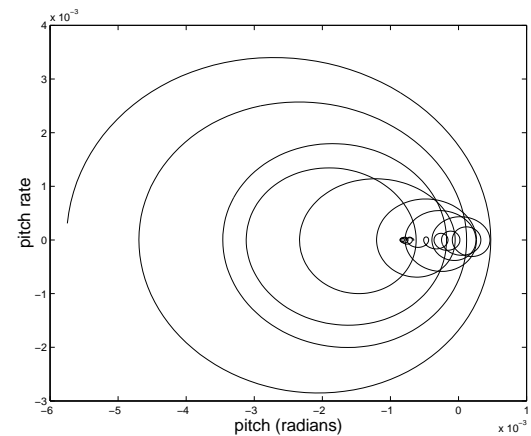


Fig. 22 Phase plane without polynomial structural nonlinearity, $M = 0.85$ and $U^* = 23$.

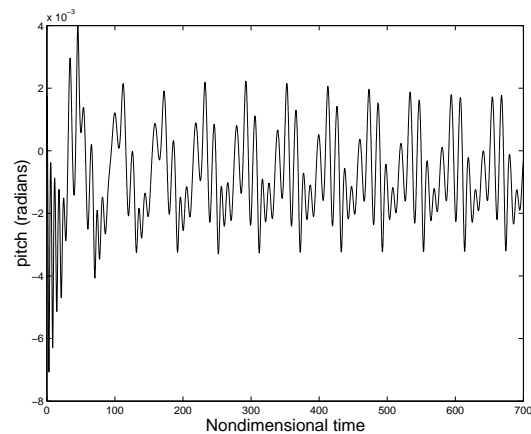


Fig. 23 Time history with polynomial structural nonlinearity, $M = 0.85$ and $U^* = 2$.

CFD and structural method provides the

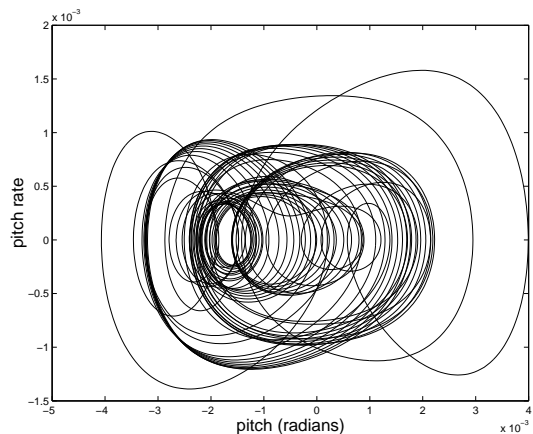


Fig. 24 Phase plane with polynomial structural nonlinearity, $M = 0.85$ and $U^* = 23$.

time history of bending and torsional motion for a NACA0012 airfoil. The results has been analysed from time histories and phase planes. For Mach number 0.85 with linear strutre the results have shown different modes and amplitude of oscillations. When reduced velocity increased from 10 to nearly 75, where a strong divergence condition is exceeded. Adding polynomial structural nonlinearity to a typical section model in transonic flow has shown destabilizing effects in the converged response and higher frequency in the limit cycle oscillation response. These tests cases have presented the capability of the integrate CFD and structural program to predict LCO. Then, the preliminary results obtained encourage the authors to move forward to verify of the methodology proposed.

Once validated, this metodology will provide the required capabilities to study aeroelastic stability problems using modern CFD codes. During this development, Hopf bifurcation analysis for flutter boundary on transonic flow will be considered. This work developments will provide the basis for further advance to complete analysis of stability and bifurcation like LCO and chaos on transonic regime.

References

[1] Alonso, J. J. and Jameson, A., "Fully-implicit time-marching aeroelastic solutions", 32nd

AIAA, Aerospace Sciences Meeting Exhibit, 32 nd, Reno, NV, 10-13 January 1994.

[2] Azevedo, J.L.F., "On The Development of Unstructured Grid Finite Volume Solver for High Speed Flows", *Report NT-075-ASE-N/92*, Instituto de Aeronáutica e Espaço, São José dos Campos, SP, Brazil, 1992.

[3] Badcock, K. J.; Woodgate, M. A.; Richards, B. E., "Hopf Bifurcation Calculations for Symmetric Airfoil in Transonic Flow", *AIAA Journal*, vol. 42, n. 5, pp. 883-892, May 2004.

[4] Badcock, K. J.; Woodgate, M. A.; Richards, B. E., "Direct Aeroelastic Bifurcation Analysis of a Simmetric Wing Based on Euler Equations", *Journal of Aircraft*, vol. 42, n. 3, May-June 2005.

[5] Bigarella, E. D. V.; Basso, E.; Azevedo, J. L. F., "Cetered and Upwind Multigrid Turbulent Flow Simulations with Applications to Launch Vehicles", AIAA Paper 2004-5384, 22nd AIAA Applied Aerodynamics Conference and Exhibit, Providence, RI, Aug 2004.

[6] Bisplinghoff, R. L. and Ashley, H. and Halfman, R. L., "*Aeroelasticity*", Dover - New York, 1996.

[7] Bunton, R. W. and Denegri, C. M., "Limit cycle oscillation characteristics of fighter aircraft", *Journal of Aircraft*, vol. 37, n. 5, pp. 916-918, 2000.

[8] Denegri, C. M., Jr., "Limit cycle oscillation flight test results of a fighter with external stores", *Journal of Aircraft*, vol. 37, n.5, pp. 761-769, 2000.

[9] Dowell, E. H. and Tang, D., "Nonlinear aeroelasticity and unsteady aerodynamics", *AIAA Journal*, vol. 40, n. 9, pp. 1697-1707, 2002.

[10] Dowell, E. H. and Tang, D. and Strganac, T. W., "Nonlinear aeroelasticity", *Journal of Aircraft*, Vol. 40, n. 5, pp. 857-874, 2003.

[11] Dubuc L.; Cantarini F.; Woodgate, M. A.; Gribben B.; Badcock, K. J.; Richards, B. E., "Solution of the Euler Unsteady Equation Using Deforming Grids", Glasgow University Department of Aerospace Engineering, Report 9704, 1997.

[12] Jameson, A. and Schmidt, W. & Turkel, E., "Numerical simulation of the euler equation by finite volume using Runge-Kutta time stepping

- schemes", AIAA Paper, pp. 81-1259, 1981.
- [13] Kholodar, D. B. K. and Thomas, J. P. and Dowell, E. H. and Hall, K. C., "Parametric study of flutter for an airfoil in inviscid transonic flow", *Journal of Aircraft*, vol. 40, n. 2, pp. 303-313, Mar-Apr 2003.
- [14] Kousen, K. A. and Bendiksen, O. O., "Limit cycle phenomena in computational transonic aeroelasticity", *Journal of Aircraft*, vo. 32, n. 2, pp. 1257-1263, 1994.
- [15] Ko, J. and Kurdila, A. J. and Strganac, T. W., "Nonlinear dynamics and control for a structurally nonlinear aeroelastic system", Published by the American Institute of Aeronautics and Astronautics, 1997.
- [16] Lee, B. H. K. and Price, S. J. and Wong, Y. S., "Nonlinear aeroelastic analysis of airfoils: bifurcation and chaos", *Progress in Aerospace Sciences*, Vol.35, pp. 205-334, 1999.
- [17] Liu, F. and Cai, J. and Zhu, Y. and Tsai, H. M. and Wong, A. S. F., "Calculation of wing flutter by a coupled fluid-structure method", *Journal of Aircraft*, vol. 38, n. 2, pp. 334-342, Mar-Apr 2001.
- [18] Oliveira, L. C., "A state-space aeroelastic analysis methodology using computational aerodynamics techniques", Master Thesis - Instituto Tecnológico de Aeronáutica, São José dos Campos, S. P., Brazil, 1993 (in Portuguese).
- [19] Simões, C. F. C.; Azevedo, J. L. F., "The influence of numerical parameters on unsteady airfoil inviscid flow simulations using unstructured dynamic meshes", *Brazilian Progress in Aerospace Engineering*, Águas de Lindóia, São Paulo, Brazil, 22-26 Nov 1999.
- [20] Thomas, J. P. and Dowell, E. H. and Hall, K. C., "Nonlinear inviscid aerodynamic effects on transonic divergence, flutter, and limit-cycle oscillations", *AIAA Journal*, vol. 40, n. 4, pp. 638-646, 2002.